Supporting information

Direct Z-Scheme Heterojunction of Semicoherent $FAPbBr_3/Bi_2WO_6$ Interface for Photoredox Reaction with Large Driving Force

Haowei Huang,[†] Jiwu Zhao,[‡] Yijie Du,[♯] Chen Zhou,[⁋] Menglong Zhang,[§] Zhuan Wang,[♯] Yuxiang Weng,[♯] Jinlin Long,[‡]* Johan Hofkens,[∥] Julian A. Steele,[†]* and Maarten B. J. Roeffaers[†]*

† cMACS, Department of Microbial and Molecular Systems, KU Leuven, Celestijnenlaan 200F, 3001 Leuven, Belgium

‡ State Key Laboratory of Photocatalysis on Energy and Environment, Fuzhou University, Fuzhou 350002, China

♯ Laboratory of Soft Matter and Biophysics, Institute of Physics, Chinese Academy of Sciences, Beijing 100190, China

⁋ College of Chemical Engineering, Fuzhou University, Fuzhou 350002, China

§ Institute of Semiconductors, South China Normal University, Guangzhou, 510631 China

∥ Department of Chemistry, KU Leuven, Celestijnenlaan 200F, 3001 Heverlee, Belgium; Max Planck Institute for Polymer Research, Ackermannweg 10, 55128 Mainz, Germany

Email: jllong@fzu.edu.cn, julian.steele@kuleuven.be, maarten.roeffaers@kuleuven.be

Supporting Figures

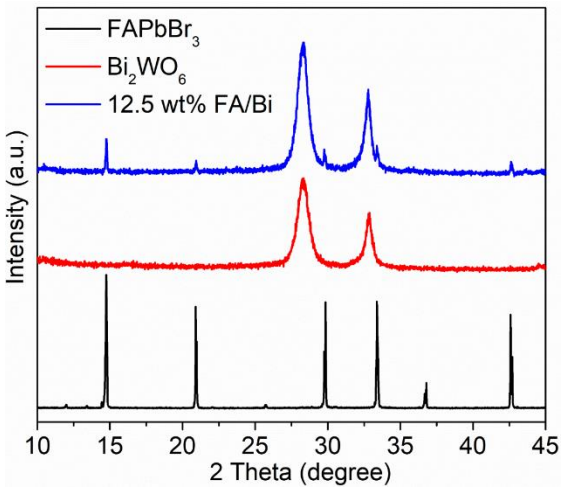

Figure S1. XRD patterns of $FAPbBr_3$, Bi_2WO_6 and 12.5% $FAPbBr_3/Bi_2WO_6$(FA/Bi).

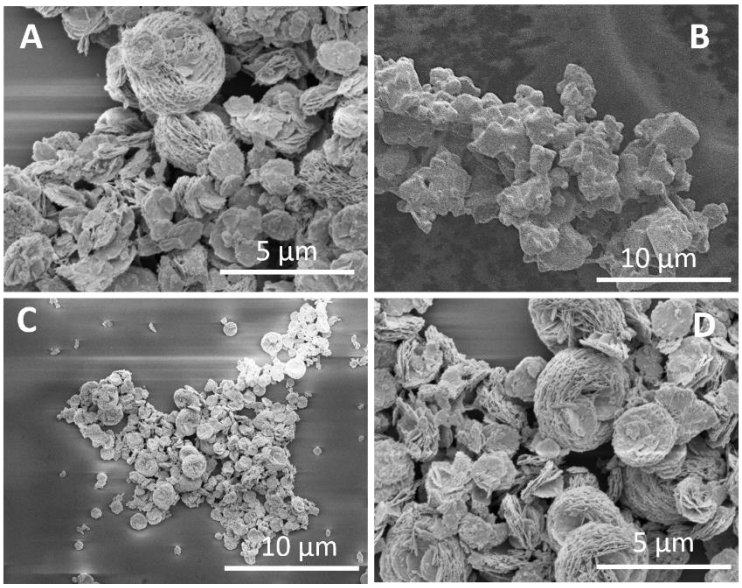

Figure S2. SEM patterns of (A) Bi_2WO_6, (B) $FAPbBr_3$, (C) and (D)12.5% $FAPbBr_3/Bi_2WO_6$

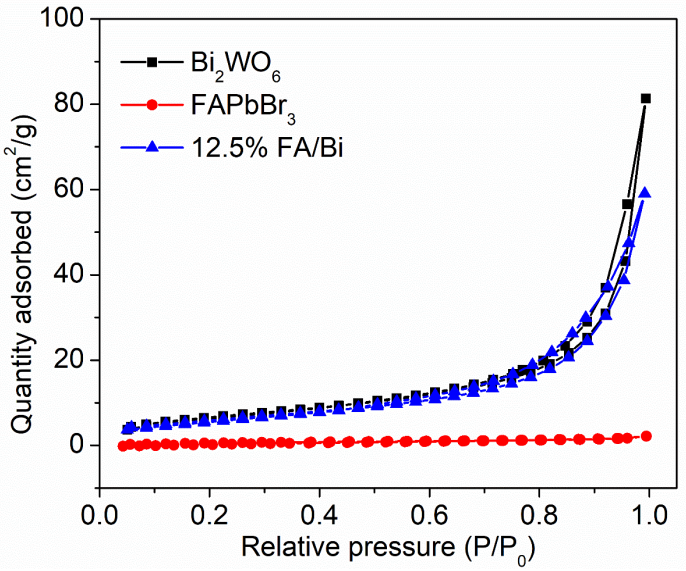

Figure S3. N_2 adsorption-desorption isotherms of of Bi_2WO_6, $FAPbBr_3$, and 12.5% $FAPbBr_3/Bi_2WO_6$(FA/Bi).

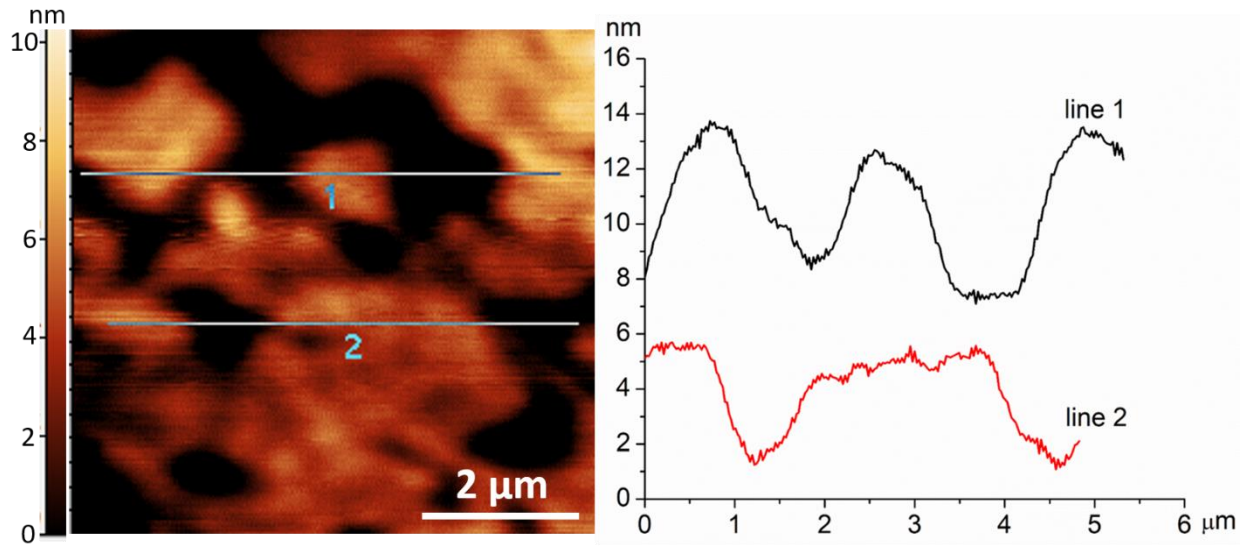

Figure S4. AFM micrograph of Bi_2WO_6, and the corresponding height profiles.

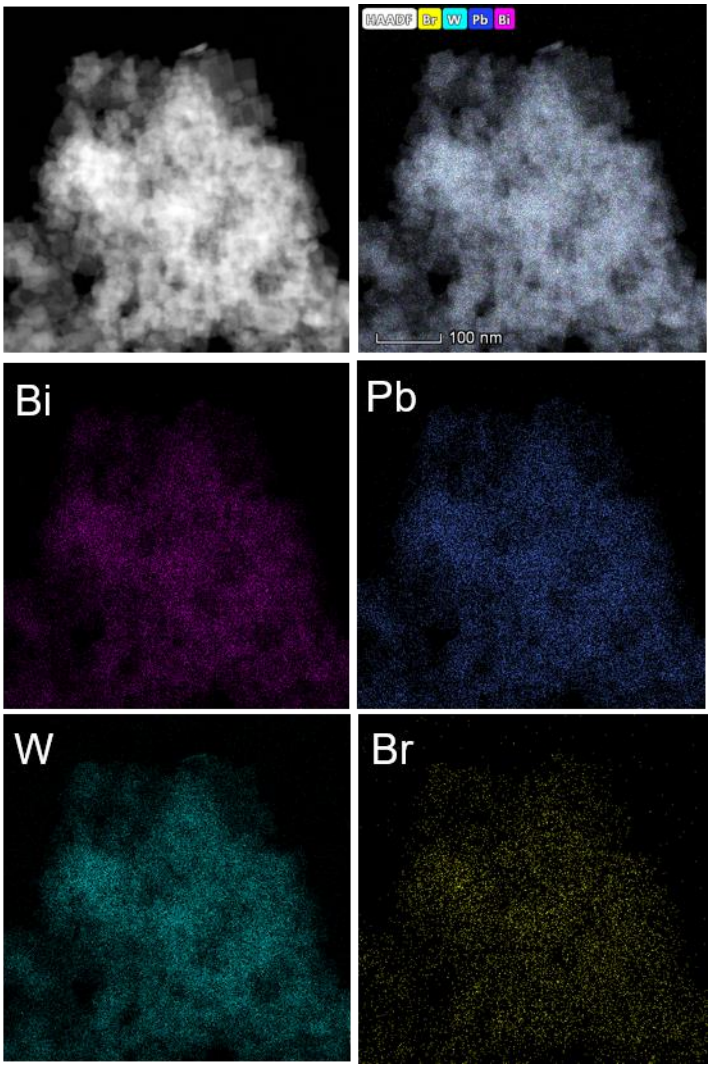

Figure S5. Elemental mapping pattern of the 12.5% $FAPbBr_3/Bi_2WO_6$ photocatalyst. Based on the EDX element mapping pattern, we further confirm the distribution relationship and intimate contact of these two components.

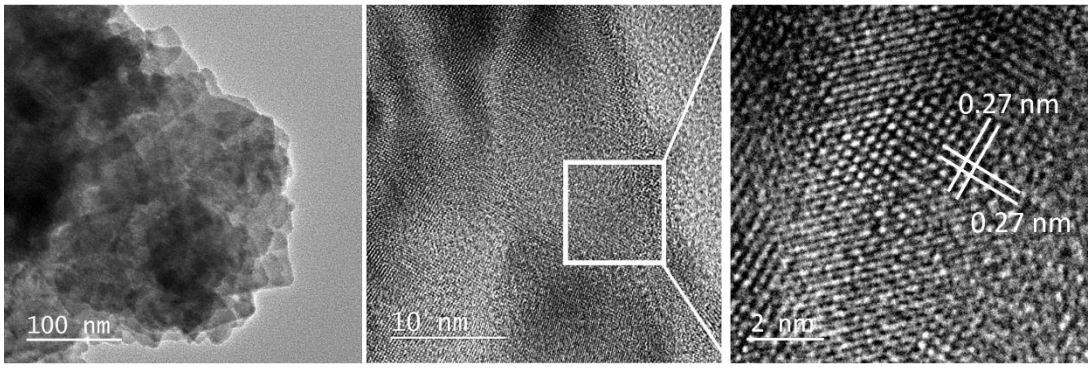

Figure S6. TEM and HRTEM pattern of Bi_2WO_6.

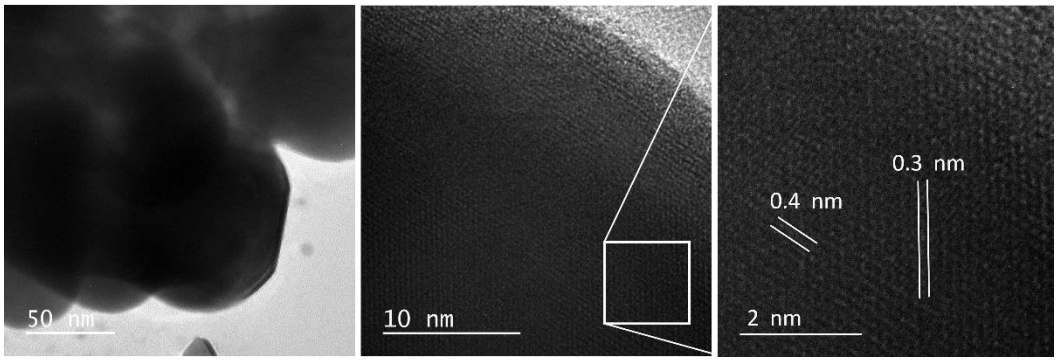

Figure S7. TEM and HRTEM pattern of $FAPbBr_3$.

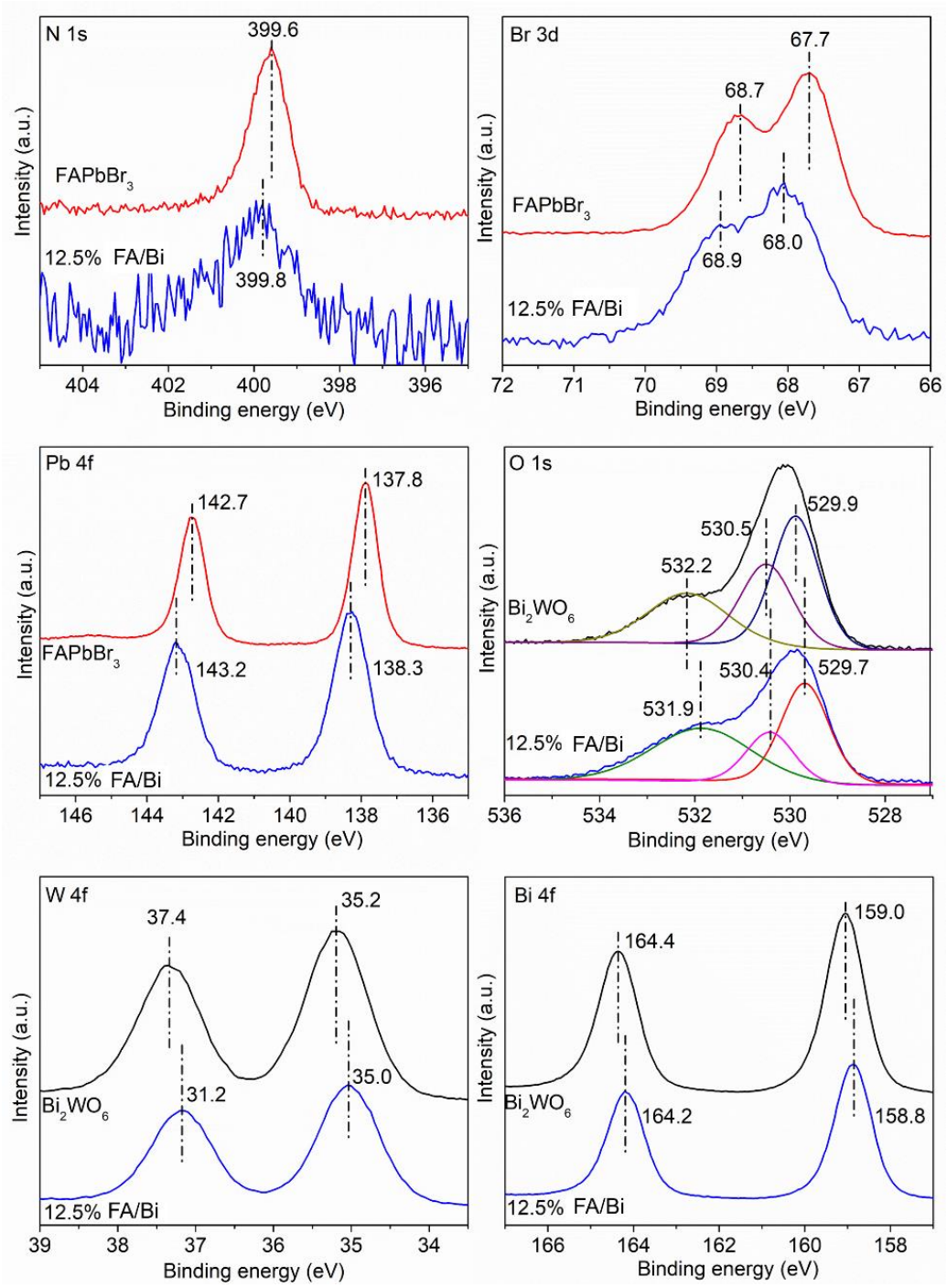

Figure S8. XPS spectra of N 1s, Br 3d and Pb 4f and in $FAPbBr_3$ and 12.5% $FAPbBr_3/Bi_2WO_6$ and O1s, W4f and Bi4f in Bi_2WO_6 and 12.5% $FAPbBr_3/Bi_2WO_6$.

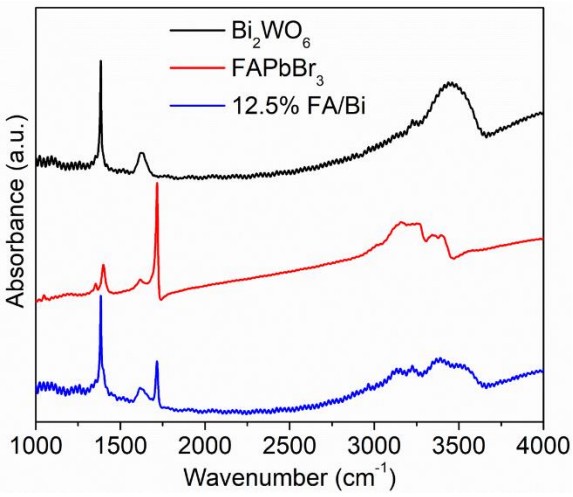

Figure S9. FTIR spectra of Bi_2WO_6, $FAPbBr_3$ and 12.5% $FAPbBr_3/Bi_2WO_6$.

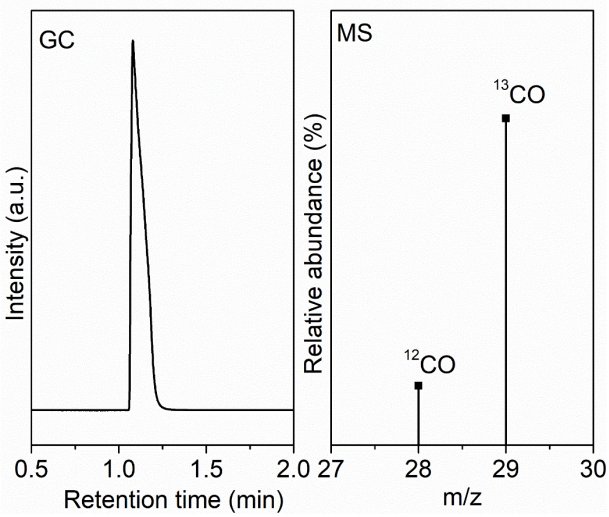

Figure S10. Results of GC-MS analysis of the CO generated from $^{13}CO_2$ isotope experiment.

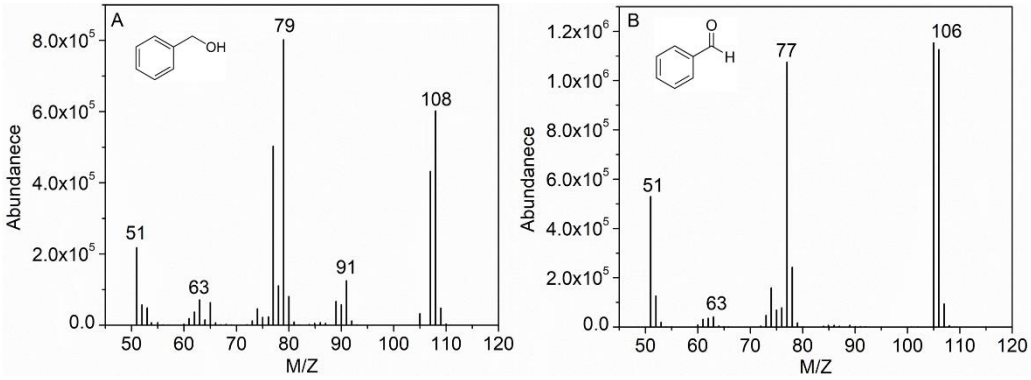

Figure S11. Mass spectra of benzyl alcohol and benzaldehyde.

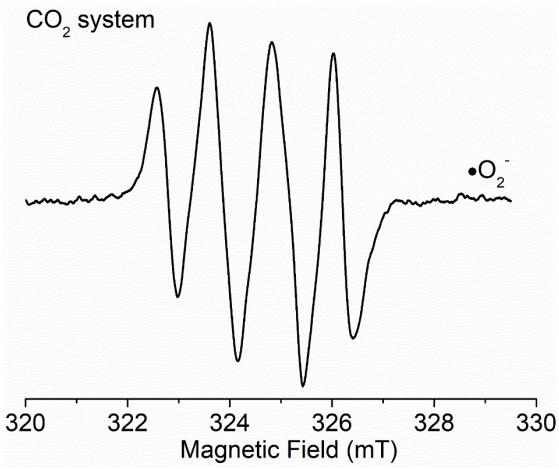

Figure S12. DMPO-trapped superoxide radical of 12.5% $FAPbBr_3/Bi_2WO_6$ in CO_2 flashed trifluorotoluene.

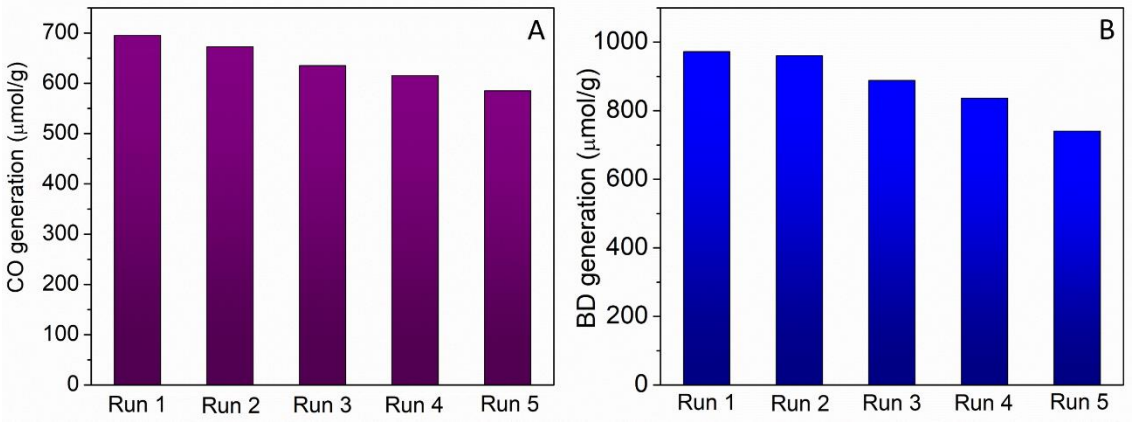

Figure S13. Recycle test for 12.5% $FAPbBr_3/Bi_2WO_6$. Reaction conditions: benzyl alcohol (0.1 mmol), photocatalysts (0.01 g), solvent of trifluorotoluene (2.5 mL) saturated with CO_2, AM1.5G simulated light irradiation, 100mW/cm^2, irradiation time (4 h). The stability of this Z-scheme photocatalyst was validated during a recycling test where the 12.5 wt% $FAPbBr_3/Bi_2WO_6$ during five consecutive reaction cycles (20h in total) showed less than 20 % activity loss. This loss in activity is linked to the decomposition of the $FAPbBr_3$ exposed to the generated BD, water and light irradiation.[1,2] The XRD is employed for the used $FAPbBr_3/Bi_2WO_6$ samples. (Figure S13). We remain optimistic that the design of future photocatalyst cells will ultimately resolve this problem *via* all-inorganic perovskite Z scheme photocatalyst such as $CsPbBr_3/Bi_2WO_6$, the use of microflow reactor and/or perovskite surface passivating molecules.

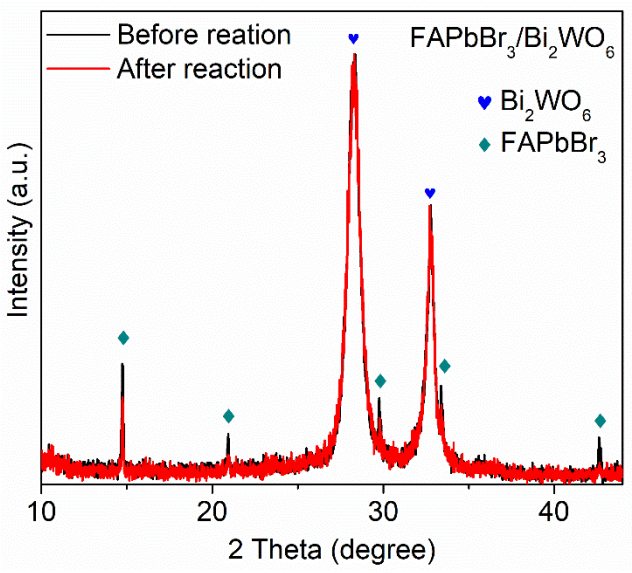

Figure S14. XRD pattern of 12.5% $FAPbBr_3/Bi_2WO_6$ after 5 cycle reaction (20h). no any new peak will appearance in the XRD pattern, but the intensity of the peaks belonging to $FAPbBr_3$ is weaker.

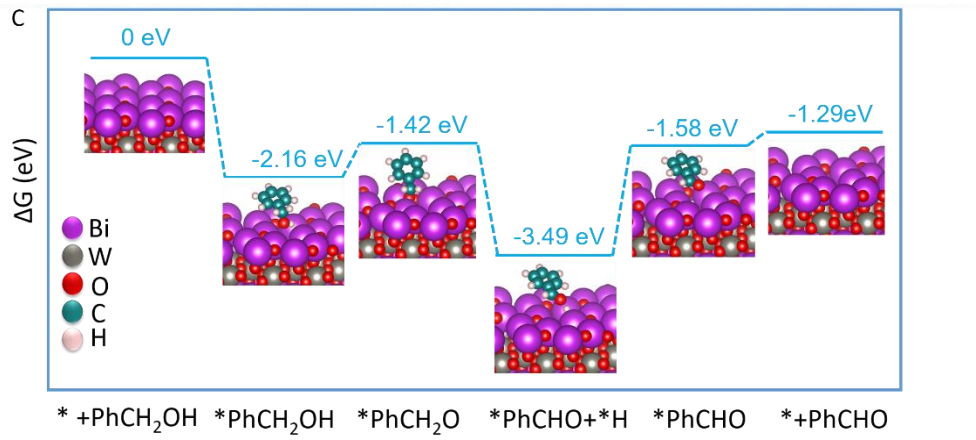

Figure S15. The DFT calculated potential energy diagram of benzyl alcohol oxidation on Bi_2WO_6.

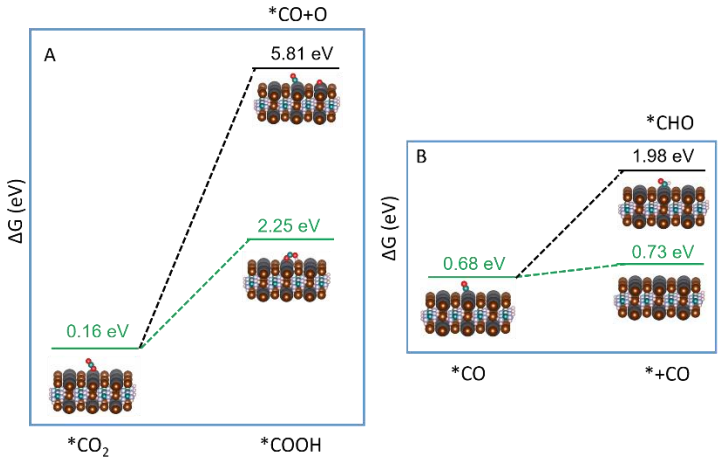

Figure S16. Steps are crucial to determining the reaction pathway(A) and selectivity(B) to CO for $FAPbBr_3/Bi_2WO_6$.

Tables

Table S1 BET surface area of Bi_2WO_6, $FAPbBr_3$ and 12.5% $FAPbBr_3/Bi_2WO_6$.

Sample	BET surface area (m^2/g)
Bi_2WO_6	25.4
$FAPbBr_3$	2.7
12.5% $FAPbBr_3/Bi_2WO_6$	22.3

Table S2. The fit results of fs-ps IR kinetic traces of Bi_2WO_6, $FAPbBr_3$ and 12.5% $FAPbBr_3/Bi_2WO_6$ at 2090 cm^{-1} excited by 470 nm pump light.

Sample	A_1/τ_1(ps)	A_2/τ_2(ps)
Bi_2WO_6	-	-
$FAPbBr_3$	0.55/4.4	0.45/48.2
$FAPbBr_3/Bi_2WO_6$	0.81/16.6	0.3/144.6

Table S3. The fit results of the raising phase in fs-ps IR kinetic traces of Bi_2WO_6, $FAPbBr_3$ and 12.5% $FAPbBr_3/Bi_2WO_6$ at 2090 cm^{-1} excited by 360 and 470 nm pump light. Here '*' indicates the injection process if too fast to be resolved reliably.

Sample	τ_{rise} (360nm)	τ_{rise} (470nm)
Bi_2WO_6	*	NA
$FAPbBr_3$	0.17	0.07 ps
$FAPbBr_3/Bi_2WO_6$	0.12	0.8 ps

Table S4. The fit results of fs-ps IR kinetic traces of Bi_2WO_6, $FAPbBr_3$ and 12.5% $FAPbBr_3/Bi_2WO_6$ at 2090 cm^{-1} excited by 360 nm pump light.

Sample	A_1/τ_1(ps)	A_2/τ_2(ps)	A_3/τ_3(ns)
Bi_2WO_6	0.000474/3.45	0.000227/95.2	-/>3
$FAPbBr_3$	0.008175/3.39	0.004996/34.3	-/>3
$FAPbBr_3/Bi_2WO_6$	0.000731/3.44	0.000281/66.6	-/>3

Table S5. The fit results of ns-μs IR kinetic traces of Bi_2WO_6, $FAPbBr_3$ and 12.5% $FAPbBr_3/Bi_2WO_6$ at 2090 cm^{-1} excited by 360 nm pump light.

Sample	A_1/τ_1(μs)	A_2/τ_2(μs)	A_3/τ_3(ms)
Bi_2WO_6	-	0.579/34.0	0.424/1.07
$FAPbBr_3$	-	-	0.799/1.53
$FAPbBr_3/Bi_2WO_6$	0.106/5.9	0.249/47.0	0.663/1.99

Table S6. The amount of CO and benzaldehyde generation in different conditions.

Sample	CO evolution rate (μmol/g/h)	Benzaldehyde (μmol/g/h)	Reaction condition
$FAPbBr_3$	12	18	AM1.5 filter, 100mW/cm^2, CO_2, benzyl alcohol
$FAPbBr_3$	10	16	AM1.5 filter, 100mW/cm^2, Ar, benzyl alcohol
$FAPbBr_3$	<5	<5	CO_2, benzyl alcohol, without light,
$FAPbBr_3$	11	<5	AM1.5 filter, 100mW/cm^2, Ar, no benzyl alcohol
Bi_2WO_6	<5	63	AM1.5 filter, 100mW/cm^2, CO_2, benzyl alcohol
$FAPbBr_3/Bi_2WO_6$	170	250	AM1.5 filter, 100mW/cm^2, CO_2, benzyl alcohol
$FAPbBr_3/Bi_2WO_6$	<5	<5	CO_2, benzyl alcohol, without light
$FAPbBr_3/Bi_2WO_6$	13	<5	AM1.5 filter, 100mW/cm^2, Ar, no benzyl alcohol
$FAPbBr_3/Bi_2WO_6$	15	<5	AM1.5 filter, 100mW/cm^2, CO_2, no benzyl alcohol
$FAPbBr_3/Bi_2WO_6$	12	130	AM1.5 filter, 100mW/cm^2, Ar, benzyl alcohol
$FAPbBr_3/Bi_2WO_6$	-	580	AM1.5 filter, 100mW/cm^2, O_2, benzyl alcohol

Table S7. Photocatalytic reduction CO_2 to fuels over various photocatalysts under different experimental conditions.

Sample	Production(production rate (μmol/g/h))	Reaction condition	Reference
$FAPbBr_3/Bi_2WO_6$	CO(170)	AM1.5G fliter, 100mW/cm^2	This work
$CsPbBr_3$ QD	CO(4.2) CH_4(1.9)	100-W Xe lamp, AM 1.5G filter	[3]
$CsPbBr_3$ QD/GO	CO(5) CH_4(2.5)	100-W Xe lamp, AM 1.5G filter	[3]
$Cs_2AgBiBr_6$	CO(2.35) CH_4(1.6)	AM 1.5G filter, 150 mW/cm^2	[4]
$CsPb(Br_x/Cl_{1-x})_3$	CO(87) CH_4(12)	300 W Xe lamp.AM 1.5G filter	[5]
$CsPbBr_3$ QDs/UiO-66(NH2)	CO(8)	300 W Xe lamp, 420nm cut-off	[6]
$CsPbBr_3$ NC/a-TiO_2	CO(7) CH_4(4)	AM 1.5G filter, 150 mW/cm^2	[7]
$CsPbBr_3$@ZIF-67	CO(1) CH_4(3)	AM 1.5G, 150 mW/cm^2	[8]
CsPbBr3 QDs/g-C3N4	CO(148.9)	300 W Xe lamp, 420 nm cut-off	[9]
$CsPbBr_3$/ZnO/GO	CO(1) CH_4(6)	AM 1.5G, 150 mW/cm^2	[10]
MAPbI3@PCN-221(Fe0.2)	CO(4.16) CH_4(13)	300 W Xe lamp, 100 mW/cm^2	[11]
Cs_2SnI_6/SnS_2	CH_4(6.09)	150 mW/cm^2, 400 nm filter	[12]

Reference

(1) Huang, H.; Yuan, H.; Janssen, K. P. F.; Solís-Fernández, G.; Wang, Y.; Tan, C. Y. X.; Jonckheere, D.; Debroye, E.; Long, J.; Hendrix, J.; Hofkens, J.; Steele, J. A.; Roeffaers, M. B. J. Efficient and Selective Photocatalytic Oxidation of Benzylic Alcohols with Hybrid Organic–Inorganic Perovskite Materials. *ACS Energy Lett.* **2018**, *3*, 755-759.

(2) Huang, H.; Yuan, H.; Zhao, J.; Solís-Fernández, G.; Zhou, C.; Seo, J. W.; Hendrix, J.; Debroye, E.; Steele, J. A.; Hofkens, J.; Long, J.; Roeffaers, M. B. J. C(sp3)–H Bond Activation by Perovskite Solar Photocatalyst Cell. *ACS Energy Lett.* **2018**, *4*, 203-208.

(3) Xu, Y. F.; Yang, M. Z.; Chen, B. X.; Wang, X. D.; Chen, H. Y.; Kuang, D. B.; Su, C. Y. A CsPbBr3 Perovskite Quantum Dot/Graphene Oxide Composite for Photocatalytic CO_2 Reduction. *J. Am. Chem. Soc.* **2017**, *139*, 5660-5663.

(4) Zhou, L.; Xu, Y.-F.; Chen, B.-X.; Kuang, D.-B.; Su, C.-Y. Synthesis and Photocatalytic Application of Stable Lead-Free Cs2AgBiBr6 Perovskite Nanocrystals. *Small* **2018**, *14*, 1703762.

(5) Guo, S.-H.; Zhou, J.; Zhao, X.; Sun, C.-Y.; You, S.-Q.; Wang, X.-L.; Su, Z.-M. Enhanced CO_2 Photoreduction *via* Tuning Halides in Perovskites *J. Catal.* **2019**, *369*, 201-208.

(6) Wan, S.; Ou, M.; Zhong, Q.; Wang, X. Perovskite-Type Cspbbr$_3$ Quantum Dots/Uio-66(NH_2) Nanojunction as Efficient Visible-Light-Driven Photocatalyst for CO_2 Reduction. *Chem. Engineer.J.* **2019**, *358*, 1287-1295.

(7) Xu, Y.-F.; Wang, X.-D.; Liao, J.-F.; Chen, B.-X.; Chen, H.-Y.; Kuang, D.-B. Amorphous‐TiO_2-Encapsulated $CsPbBr_3$ Nanocrystal Composite Photocatalyst with Enhanced Charge Separation and CO_2 Fixation. *Adv. Mater. Interfaces* **2018**, *5*, 1801015

(8) Kong, Z.-C.; Liao, J.-F.; Dong, Y.-J.; Xu, Y.-F.; Chen, H.-Y.; Kuang, D.-B.; Su, C.-Y. Core@Shell $CsPbBr_3$@Zeolitic Imidazolate Framework Nanocomposite for Efficient Photocatalytic CO_2 Reduction. *ACS Energy Lett.* **2018**, *3*, 2656-2662.

(9) Ou, M.; Tu, W.; Yin, S.; Xing, W.; Wu, S.; Wang, H.; Wan, S.; Zhong, Q.; Xu, R. Amino-Assisted Anchoring of $CsPbBr_3$ Perovskite Quantum Dots on Porous g-C3N4 for Enhanced Photocatalytic CO_2 Reduction *Angew. Chem.* **2018**, *130*, 13758-13762.

(10) Jiang, Y.; Liao, J.-F.; Xu, Y.-F.; Chen, H.-Y.; Wang, X.-D.; Kuang, D.-B. Hierarchical $CsPbBr_3$ Nanocrystal-Decorated ZnO Nanowire/Macroporous Graphene Hybrids for Enhancing Charge Separation and Photocatalytic CO_2 Reduction. *J. Mater. Chem. A* **2019**, *7*, 13762-13769.

(11) Wu, L.-Y.; Mu, Y.-F.; Guo, X.-X.; Zhang, W.; Zhang, Z.-M.; Zhang, M.; Lu, T.-B. Encapsulating Perovskite Quantum Dots in Iron-Based Metal-Organic Frameworks (MOFs) for Efficient Photocatalytic CO_2 Reduction. *Angew. Chem. Int. Ed.*, **2019**, *58*, 9491-9495.

(12) Wang, X.-D.; Huang, Y.-H.; Liao, J.-F.; Jiang, Y.; Zhou, L.; Zhang, X.-Y.; Chen, H.-Y.; Kuang, D.-B. *In Situ* Construction of a Cs_2SnI_6 Perovskite Nanocrystal/SnS_2 Nanosheet Heterojunction with Boosted Interfacial Charge Transfer. *J. Am. Chem. Soc.* **2019**, *141*, 13434-13441.